Journal of Marine Science and Technology (2024) 29:641–655
https://doi.org/10.1007/s00773-024-01006-2

ORIGINAL ARTICLE

Probability density function of roll amplitude for parametric rolling using moment equation

Yuuki Maruyama[1] · **Atsuo Maki**[1] · **Leo Dostal**[2]

Received: 26 July 2023 / Accepted: 23 May 2024 / Published online: 25 July 2024

Abstract
For the ship stability estimation and ship design, it is helpful to know the probability of the roll amplitude exceeding a certain threshold. Therefore, it is necessary to obtain the probability density function of the roll amplitude. In this study, first, we derive the moment values of roll amplitude by combining the moment equations and the linearity of expectation. With this, we propose a method to estimate the probability density function of the roll amplitude by using the obtained moment values. The results of our proposed method are compared to those obtained from Monte Carlo simulations. When the higher-order cumulant neglect closure method is used, the moment values resulting from the moment equations are close to the results of corresponding Monte Carlo simulations. In addition, our proposed method for deriving the probability density function of the roll amplitude is validated by comparison with Monte Carlo simulation results. In conclusion, we can state that the proposed methods for deriving the moments and the probability density function of the roll amplitude are available for practical use cases.

Keywords Parametric rolling · Moment equation · Roll amplitude · Probability density function

1 Introduction

Parametric rolling is a known phenomenon of roll motion which is induced by a time-varying restoring arm. In particular, this phenomenon tends to occur when the natural roll frequency is about twice the encounter wave frequency. In October 1998, a C11 class post-Panamax container ship encountered a violent storm in the North Pacific Ocean. According to a report [1], a heel angle of 35° to 40° occurred in head seas, and one-third of the approximately 1300 containers on deck were lost to the ocean and another one-third were damaged. In another incident, an accident of a car and truck carrier vessel occurred due to violent roll motion in rough head seas while the ship was traveling in the Atlantic Ocean in February 2003 [2, 3]. As a consequence, the International Maritime Organization developed and circulated an interim guideline on second-generation intact stability criteria for five dangerous phenomena including parametric rolling [4]. Later, the explanatory notes were finalized in 2022 [5].

For ship stability estimation and ship design, it is useful to consider the roll amplitude rather than an instantaneous value such as the roll angle. Hashimoto and Umeda [6] and Sakai et al. [7] applied the averaging method and analytically obtained the roll amplitude. Also, Maki et al. [8] analyzed the method by combining deterministic and stochastic approaches. For the estimation, it is desirable to have a method that analytically derives the probability exceeding a certain threshold. Much research has been conducted on the derivation of the probability density function (PDF) of the roll amplitude by using the stochastic approach. Ariaratnam and Tam [9], and Roberts [10] applied the stochastic averaging method to the one-degree-of-freedom stochastic oscillator with linear restoring, which can be used as a model of roll motion. They derived stochastic differential equations (SDE) of the roll amplitude and phase based on the limit theorem proposed by Stratonovich [11] and Khasminskii [12]. In this method, a colored noise random process is considered. However, this stochastic averaging method separates the damping and restoring components

✉ Yuuki Maruyama
yuuki_maruyama@naoe.eng.osaka-u.ac.jp

[1] Department of Naval Architecture and Ocean Engineering, Graduate School of Engineering, Osaka University, 2-1 Yamadaoka, Suita, Osaka, Japan

[2] Institute of Mechanics and Ocean Engineering, Hamburg University of Technology, 21043 Hamburg, Germany

to SDEs of amplitude and phase, respectively. Thereby, the PDF of the roll amplitude obtained by this method reflects the characteristic of the damping component only. In order to overcome this limitation, Roberts [13, 14] and Roberts and Spanos [15] used the energy envelope methodology. To predict the ship motion with respect to parametric rolling in irregular quartering waves, Dostal et al. [16] established the energy-based stochastic averaging method. Moreover, Maruyama et al. [17] proposed an improvement of this method.

Moreover, a method to derive the PDF of the roll angle was proposed in a previous paper [18]. In that paper, the moment values obtained by solving moment equations were used and the coefficients included in the PDF were optimized. However, the method for deriving the PDF of the roll amplitude was not investigated. Therefore the purpose of this paper is to derive the PDF of the roll amplitude. First, a linear filter is required to model the wave elevation. In order to achieve this, the results obtained from the calculations for the 2nd-, 4th-, and 6th-order linear filters are compared and discussed. Second, corresponding moment equations for the linear filter SDE are derived. Then, by applying the cumulant neglect closure method, the moment values of the roll angle and rate are determined. With this, a method to derive the moment values of the roll amplitude from the moment values of instantaneous roll angle and rate is proposed. Finally, the process of deriving the PDF of the roll amplitude is examined.

2 Subject ship

The subject ship in this study is a post-Panamax container ship of the C11 class [19]. The body plan and the principal particulars of this ship are shown in Fig. 1 and Table 1, respectively. The restoring arm is calculated based on the Froude–Krylov hypothesis [20]. The ∘ in Fig. 2 shows the GZ curve in calm water. In this study, the actual GZ is approximated by a 9th-order polynomial. This approximated curve

Table 1 Principal particulars of the subject ship at full scale

Items	C11
Length: L_{pp}	262.0 m
Breadth: B	40.0 m
Depth: D	24.45 m
Draught: d	11.5 m
Block coefficient: C_b	0.562
Metacentric height: GM	1.965 m
Natural roll period: T_ϕ	25.1 s
Bilge keel length ratio: L_{BK}/L_{pp}	0.292
Bilge keel breadth ratio: B_{BK}/B	0.0100

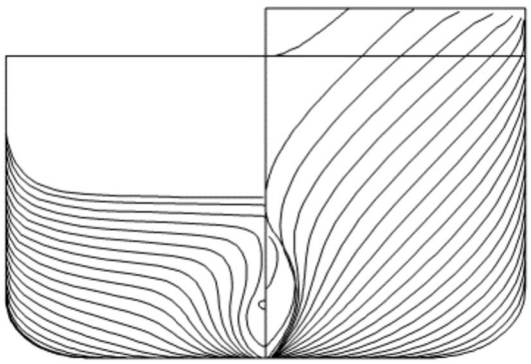

Fig. 1 Body plan (C11)

is plotted as the red solid line in Fig. 2. When the crest or trough of a regular wave with a wavelength-to-ship length ratio of 1.0 is located at amidships, the results denoted by the triangle or the cross markers in Fig. 2 are obtained by means of hydrostatic calculations. Hereby the wave steepness is 0.04. As shown in Fig. 2, the C11 container ship has a close to linear GZ curve up to a roll angle of approximately 40 degrees.

The non-memory transformation represented in Fig. 3 can be applied to generate the GM variation. This transformation links the GM variation ΔGM and the wave elevation at amidships. As mentioned earlier, the restoring arm is calculated by using the hydrodynamic theory [20]. In this study, the restoring arm is obtained for a two degrees heeling of the ship heeling in a regular wave with a wavelength-to-ship length ratio of 1.0. Additionally, the GM for each wave elevation is calculated with the wave crest or trough located at amidships. Thereby, the relationship shown in Fig. 3 is obtained. The

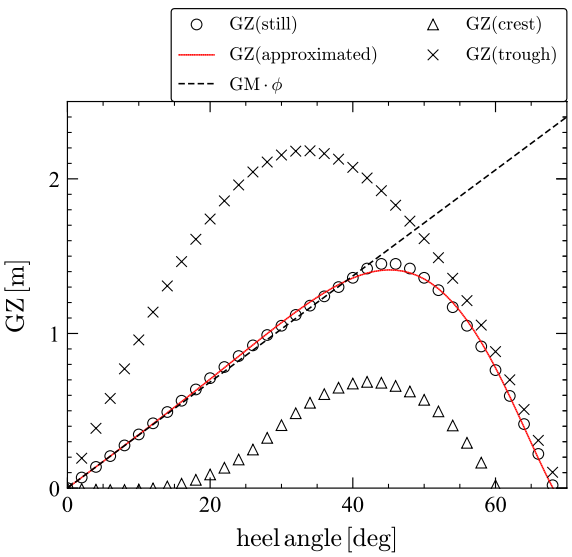

Fig. 2 GZ curve in still water (C11)

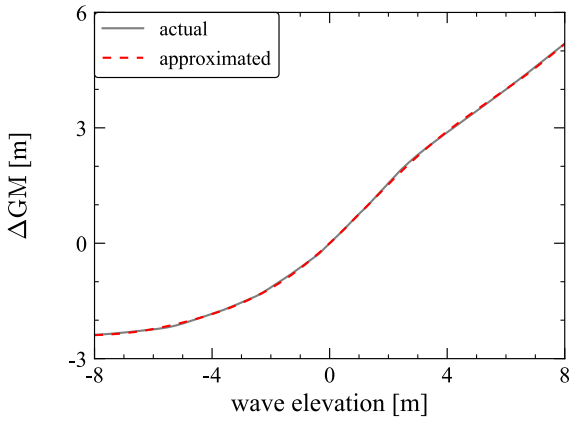

Fig. 3 Relationship between ΔGM and wave elevation amidships, subject ship: C11

wave elevation is positive when the wave trough is located at amidships and is negative when the wave crest is located at amidships. In this study, the actual data plotted as the gray solid line in Fig. 3 is approximated by a 12th-order polynomial. The red dashed line in Fig. 3 indicates this approximated curve, which fits the actual data well.

Ikeda's simplified method [21] is used to estimate the roll damping coefficients. As a result, the damping coefficients are $\beta_1 = 3.64 \times 10^{-3}\,\mathrm{rad/s}$ and $\beta_3 = 4.25\,\mathrm{s/rad^2}$.

3 Linear filter

When ocean waves are modeled by real noise, the forcing due to waves is not white noise but colored noise. In our study, a linear filter is used to generate colored noise from white noise. Spanos [22, 23], Flower and Vijeh [24, 25], and Thampi and Niedzwecki [26] applied a linear filter to the wave spectrum and showed that it can be approximated by an Autoregressive Moving Averaging (ARMA) spectrum. Recently, Maruyama et al. [18] reported that the time series of effective wave elevation can be modeled by applying a 6th-order linear filter to the effective wave spectrum.

By using a higher-order linear filter, the number of parameters in the linear filter increase. Thereby, compared to a lower-order linear filter, a better approximation can be obtained. In this study, the 2nd, 4th, and 6th-order linear filters are compared. First, the ordinary differential equations of the 2nd, 4th, and 6th-order linear filters are represented as Eqs. (1) to (3). The notation for differentiation is represented by Lagrange's notation.

$$\text{2nd:}\quad x_1'' + \alpha_1 x_1' + \alpha_2 x_1 = \Gamma\sqrt{\pi}\{W'\}' \tag{1}$$

$$\text{4th:}\quad x_1^{(4)} + \alpha_1 x_1''' + \alpha_2 x_1'' + \alpha_3 x_1' + \alpha_4 x_1 = \Gamma\sqrt{\pi}\{W'\}'' \tag{2}$$

$$\text{6th:}\quad x_1^{(6)} + \alpha_1 x_1^{(5)} + \alpha_2 x_1^{(4)} + \alpha_3 x_1''' + \alpha_4 x_1'' + \alpha_5 x_1' + \alpha_6 x_1 = \Gamma\sqrt{\pi}\{W'\}''' \,. \tag{3}$$

Here, W denotes the standard Wiener process. The spectra corresponding to Eqs. (1) to (3) are represented by Eqs. (4) to (6).

$$S_2(\omega) = \frac{\Gamma^2\omega^2}{(\omega^2 - \alpha_2)^2 + \alpha_1^2\omega^2} \tag{4}$$

$$S_4(\omega) = \frac{\Gamma^2\omega^4}{\left(\omega^4 - \alpha_2\omega^2 + \alpha_4\right)^2 + \left(\alpha_1\omega^3 - \alpha_3\omega\right)^2} \tag{5}$$

$$S_6(\omega) = \frac{\Gamma^2\omega^6}{\left(-\omega^6 + \alpha_2\omega^4 - \alpha_4\omega^2 + \alpha_6\right)^2 + \left(\alpha_1\omega^5 - \alpha_3\omega^3 + \alpha_5\omega\right)^2} \tag{6}$$

In this study, the ITTC spectrum is utilized as the ocean wave spectrum, which is given by:

$$S_w(\omega) = \frac{173H_{1/3}^2}{T_{01}^4\omega^5}\exp\left(-\frac{691}{T_{01}^4\omega^4}\right) \tag{7}$$

Here, T_{01} and $H_{1/3}$ are the mean wave period and the significant wave height, respectively. By applying the concept of Grim's effective wave [27] to irregular waves, the elevation of the effective wave at amidships is obtained. The reason for using the effective wave is that a regular wave with a wavelength-to-ship length ratio of 1.0 is considered for the calculation of the restoring arm in the non-memory transformation. The transfer function of the effective wave H_ζ can be represented as shown in the following equation [28].

$$H_\zeta(\omega,\chi) = H_{\zeta c}(\omega,\chi) + iH_{\zeta s}(\omega,\chi)$$

$$\begin{cases} H_{\zeta c}(\omega,\chi) = \dfrac{\dfrac{\omega^2 L}{g}\cos\chi\sin\left(\dfrac{\omega^2 L}{2g}\cos\chi\right)}{\pi^2 - \left(\dfrac{\omega^2 L}{2g}\cos\chi\right)^2} \\ H_{\zeta s}(\omega,\chi) = 0 \end{cases} \tag{8}$$

Here, ω denotes the wave frequency, χ denotes the ship's heading angle with respect to the propagating direction of the wave, g denotes the gravitational acceleration, and L

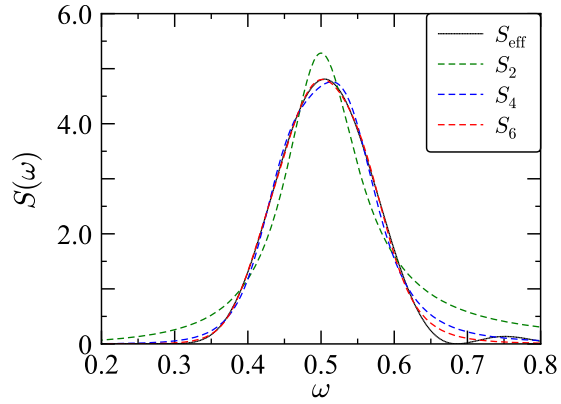

Fig. 4 Comparison among effective wave spectrum S_{eff}, 2nd-order ARMA spectrum S_2, 4th-order ARMA spectrum S_4, and 6th-order ARMA spectrum S_6. Here, the sea condition is $T_{01} = 9.99\,\mathrm{s}$ and $H_{1/3} = 5.0\,\mathrm{m}$

Table 2 Coefficients of 2nd-, 4th-, and 6th-order ARMA spectra

Coefficient	S_2	S_4	S_6
α_1	0.121	0.255	0.395
α_2	0.250	0.512	0.787
α_3	–	0.0627	0.195
α_4	–	0.0586	0.185
α_5	–	–	0.0224
α_6	–	–	0.0128
Γ	0.277	0.0613	0.0153

denotes the ship length. In the results of this study, the head seas condition ($\chi = 180$ deg) is considered. With the use of the above transfer function, the spectrum of the effective wave is obtained as follows:

$$S_{\mathrm{eff}}(\omega) = \left|H_{\zeta}(\omega)\right|^2 S_{\mathrm{w}}(\omega) \tag{9}$$

Next, the coefficients α_i and Γ of Eqs. (4) to (6) are determined such that their ARMA spectrum agrees with the effective wave spectrum. Here, the global optimization scheme CMA-ES [29] is used. The mean squared error, which is denoted by Eq. (10) is used as the objective function. Here, n denotes the total number of data points, $\hat{y}$ denotes an observed value, and y denotes a true value. This true value is given by Eq. (7).

$$J = \frac{1}{n}\sum_{i=1}^{n}\left(\hat{y}_i - y_i\right)^2 \tag{10}$$

Moreover, the stability criterion of the system proposed by Maruyama et al. [18] is used as the constraint condition.

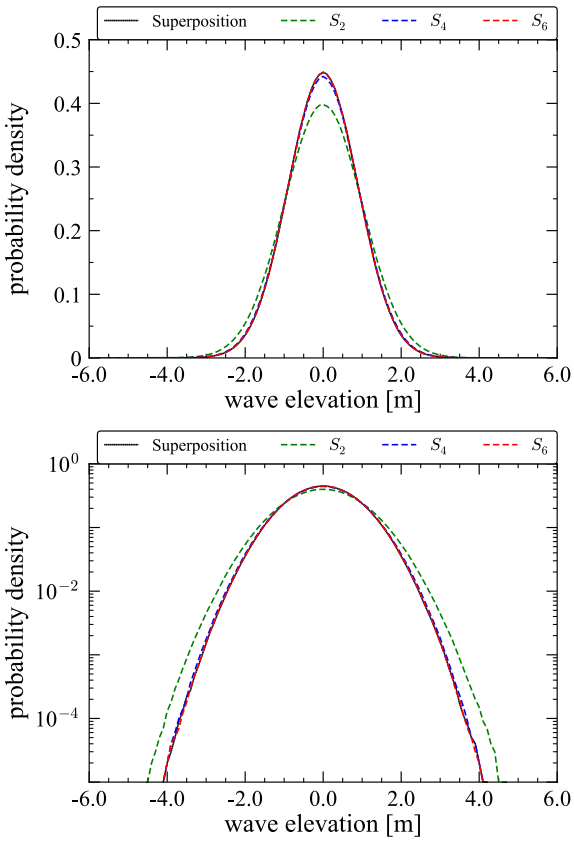

Fig. 5 Comparison of PDFs of effective wave elevation among numerical simulation by the superposition methodology: Superposition, the results obtained by solving the SDE: S_2,S_4,S_6, sea state with $T_{01} = 9.99\,\mathrm{s}$ and $H_{1/3} = 5.0\,\mathrm{m}$

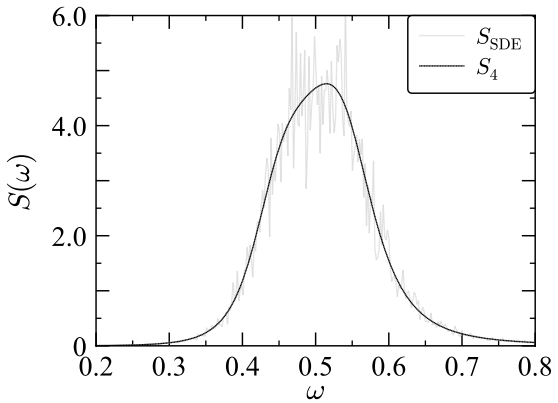

Fig. 6 Comparison between the 4th-order ARMA spectrum: S_4, and the spectrum analysis result of the time series obtained by solving the SDE: S_{SDE}, sea state with $T_{01} = 9.99\,\mathrm{s}$ and $H_{1/3} = 5.0\,\mathrm{m}$

In Fig. 4 and Table 2, we can see the calculation results of three linear filters. Adjusting the range of parameter exploration in CMA-ES, the 4th-order ARMA spectrum

Table 3 Statistical properties of the effective wave elevation PDF

	Superposition	S_2	S_4	S_6
Mean	-1.54×10^{-5}	2.74×10^{-5}	9.90×10^{-6}	2.97×10^{-5}
Variance	0.792	1.00	0.818	0.796
Skewness	2.32×10^{-4}	9.57×10^{-4}	-3.27×10^{-5}	5.28×10^{-5}
Kurtosis	3.00	3.00	2.99	2.99

is improved compared to the results shown in Maruyama et al. [18]. As shown in Figs. 5 and 6 and Table 3, although the 4th-order ARMA spectrum is less accurate than that of the 6th-order, the 4th-order ARMA spectrum can represent the effective wave elevation adequately. However, it can be observed from Fig. 4 that if the higher-order linear filter is used, the higher-order ARMA spectrum agrees well with the effective wave spectrum. To reduce the computational complexity in deriving the moment equations, the 4th-order linear filter is used in this study.

4 Moment equations

The equation for parametric rolling in longitudinal waves is given by Eq. (11).

$$\ddot{\phi} + \beta_1 \dot{\phi} + \beta_3 \dot{\phi}^3 + \omega_0^2 \sum_{n=1}^{5} \gamma_{2n-1} \phi^{2n-1} + F(A_{\mathrm{w}})\phi = 0 \tag{11}$$

where

$$F(A_{\mathrm{w}}) = \frac{\omega_0^2}{\mathrm{GM}} \sum_{n=1}^{12} \rho_n A_{\mathrm{w}}^n. \tag{12}$$

Here, ϕ and A_{w} denote the roll angle and the effective wave elevation, respectively. The parameter ω_0 denotes the natural roll frequency. Moreover, β_1 is the linear and β_3 is the cubic damping coefficient divided by I_{xx}, where I_{xx} is the moment of inertia in roll (including the corresponding added moment of inertia), $\gamma_i\,(i = 1, 3, 5, 7, 9)$ is the coefficient of the i-th component of the polynomial fitted GZ curve in Fig. 2, and $\rho_n\,(n = 1, 2, \ldots, 12)$ is the coefficient of the n-th component of the fitted polynomial for the relationship between ΔGM and wave elevation at amidships in Fig. 3. $F(A_{\mathrm{w}})$ denotes the parametric excitation process. As shown in Eq. (11), this equation is represented using the polynomial fitting.

To derive the moment equations, the system of ship motion needs to be represented by an SDE [30]. The resulting system can be expressed by means of the 6th-order Itô SDE like Eq. (13). This consists of a 2nd-order SDE for the ship motion derived from Eq. (11) and a 4th-order SDE for the effective wave elevation derived from Eq. (2).

$$\begin{cases} \mathrm{d}X_1 = X_2\,\mathrm{d}t \\ \mathrm{d}X_2 = \left\{ -G(X_1, X_2) - F(X_3)X_1 \right\}\mathrm{d}t \\ \mathrm{d}X_3 = \left(X_4 - \alpha_1 X_3 \right)\mathrm{d}t \\ \mathrm{d}X_4 = \left(X_5 - \alpha_2 X_3 \right)\mathrm{d}t + \Gamma\sqrt{\pi}\,\mathrm{d}W(t) \\ \mathrm{d}X_5 = \left(X_6 - \alpha_3 X_3 \right)\mathrm{d}t \\ \mathrm{d}X_6 = -\alpha_4 X_3 \mathrm{d}t \end{cases} \tag{13}$$

where

$$G(X_1, X_2) = \beta_1 X_2 + \beta_3 X_2^3 + \omega_0^2 \sum_{n=1}^{5} \gamma_{2n-1} X_1^{2n-1} \tag{14}$$

Here, X_1, X_2, and X_3 denote the roll angle, the roll rate, and the effective wave elevation, respectively. When an ordinary differential equation driven by Gaussian noise is transformed to an Itô SDE, the Wong-Zakai correction term has to be considered in general [31]. In this study, this correction term is zero because the diffusion coefficient, which is the coefficient of the driving noise, is not explicitly dependent on the dependent variable.

From Eq. (13), the moment equation for this system is represented as Eq. (15). Using Eq. (15), the six 1st-order, 21 2nd-order, 56 3rd-order, and 126 4th-order moment equations can be derived. Higher-order moment equations can also be derived, such as 252 5th-order and 462 6th-order moment equations, and so on. This means that an arbitrary desired number of moment equations can be generated. In general, when the system is a nonlinear system, moment equations of a specific order will contain moments of even higher order. Therefore, to form a closed set of moment equations, higher-order moments must be

truncated. To solve this problem, the cumulant neglect closure method [32] [33] [34] is used in this study. Thereby, higher-order moments can be expressed by lower-order moments. As a result, the moment equations are in a closed form, and the moment values can be computed.

$$\begin{aligned}
&\frac{\mathrm{d}}{\mathrm{d}t}\mathbb{E}\left[\prod_{k=1}^{6} X_k^{C_k}\right] \\
&= C_1\mathbb{E}\left[X_1^{C_1-1}X_2^{C_2+1}X_3^{C_3}X_4^{C_4}X_5^{C_5}X_6^{C_6}\right] \\
&- C_2\mathbb{E}\left[G(X_1,X_2)X_1^{C_1}X_2^{C_2-1}X_3^{C_3}X_4^{C_4}X_5^{C_5}X_6^{C_6}\right] \\
&- C_2\mathbb{E}\left[F(X_3)X_1^{C_1+1}X_2^{C_2-1}X_3^{C_3}X_4^{C_4}X_5^{C_5}X_6^{C_6}\right] \\
&+ C_3\mathbb{E}\left[(X_4-\alpha_1X_3)X_1^{C_1}X_2^{C_2}X_3^{C_3-1}X_4^{C_4}X_5^{C_5}X_6^{C_6}\right] \\
&+ C_4\mathbb{E}\left[(X_5-\alpha_2X_3)X_1^{C_1}X_2^{C_2}X_3^{C_3}X_4^{C_4-1}X_5^{C_5}X_6^{C_6}\right] \\
&+ C_5\mathbb{E}\left[(X_6-\alpha_3X_3)X_1^{C_1}X_2^{C_2}X_3^{C_3}X_4^{C_4}X_5^{C_5-1}X_6^{C_6}\right] \\
&- \alpha_4C_6\mathbb{E}\left[X_1^{C_1}X_2^{C_2}X_3^{C_3+1}X_4^{C_4}X_5^{C_5}X_6^{C_6-1}\right] \\
&+ \frac{\Gamma^2\pi}{2}C_4(C_4-1)\mathbb{E}\left[X_1^{C_1}X_2^{C_2}X_3^{C_3}X_4^{C_4-2}X_5^{C_5}X_6^{C_6}\right]
\end{aligned} \tag{15}$$

5 PDF of roll amplitude

The moment values can be obtained from the moment equations. However, the PDF cannot be directly obtained from the moment equations. Therefore, the derivation of the roll amplitude PDF needs further investigation. By solving the moment equations, the moment of instantaneous values, such as the roll angle, roll rate, etc., can be obtained. However, the moment value of an envelope, such as the roll amplitude, cannot be directly obtained. For this, the method for deriving the moment values of the roll amplitude from the moment of instantaneous values is investigated. First, the fundamental solution of the roll angle X_1 is defined as Eq. (16).

$$X_1 = A\cos\left(\omega_0\sqrt{\gamma_1}\,s+\theta\right) \tag{16}$$

Based on the Pythagorean trigonometric identity, the following relational expression can be derived.

$$X_1^2+\frac{X_2^2}{\omega_0^2\gamma_1}=A^2 \tag{17}$$

Next, applying the linearity of expectation, 2nd-, 4th-, and 6th-order moments of the roll amplitude can be represented as Eqs. (18) to (20).

$$\mathbb{E}\left[A^2\right]=\mathbb{E}\left[X_1^2+\frac{X_2^2}{\omega_0^2\gamma_1}\right]=\mathbb{E}\left[X_1^2\right]+\frac{1}{\omega_0^2\gamma_1}\mathbb{E}\left[X_2^2\right] \tag{18}$$

$$\begin{aligned}
\mathbb{E}\left[A^4\right]&=\mathbb{E}\left[\left(X_1^2+\frac{X_2^2}{\omega_0^2\gamma_1}\right)^2\right] \\
&=\mathbb{E}\left[X_1^4\right]+\frac{2}{\omega_0^2\gamma_1}\mathbb{E}\left[X_1^2X_2^2\right]+\frac{1}{\omega_0^4\gamma_1^2}\mathbb{E}\left[X_2^4\right]
\end{aligned} \tag{19}$$

$$\begin{aligned}
\mathbb{E}\left[A^6\right]&=\mathbb{E}\left[\left(X_1^2+\frac{X_2^2}{\omega_0^2\gamma_1}\right)^3\right] \\
&=\mathbb{E}\left[X_1^6\right]+\frac{3}{\omega_0^2\gamma_1}\mathbb{E}\left[X_1^4X_2^2\right] \\
&\quad+\frac{3}{\omega_0^4\gamma_1^2}\mathbb{E}\left[X_1^2X_2^4\right]+\frac{1}{\omega_0^6\gamma_1^3}\mathbb{E}\left[X_2^6\right]
\end{aligned} \tag{20}$$

Here, $\mathbb{E}[\cdot]$ denotes the expected value operator. These equations use two variables, such as roll angle and roll rate. Therefore, the moment values of these variables are required. For these moment values obtained by solving the moment equations, using the 2nd-order cumulant neglect closure method yields the 1st and 2nd-order moment values, and using the 3rd-order cumulant neglect closure method yields the 1st-, 2nd-, and 3rd-order moment values. Similarly, using the 4th-order cumulant neglect closure method yields the 1st-, 2nd-, 3rd-, and 4th-order moment values. Moreover, by applying the cumulant neglect closure method, the 4th- and higher-order moments included in Eqs. (19) and (20) can be obtained. Therefore, using Eqs. (18) to (20), the 2nd-, 4th-, and 6th-order moment values of the roll amplitude can be calculated. In other words, using our proposed method, the even-order moment values of the roll amplitude can be derived.

The PDF of the roll amplitude is calculated based on the resulting moment values. It has been pointed out that it is difficult to express the PDF of the roll amplitude of parametric rolling in terms of Rayleigh distribution [35]. To solve

the problem, a non-Gaussian PDF shape is defined as Eq. (21). This PDF shape is based on the PDF [36] obtained using the stochastic averaging method presented by Roberts [10]. In order to improve the fitting accuracy, the cubic term in the exponential function (d_3A^3) is added as a new term in this study.

$$\mathcal{P}(A) = \frac{C}{A^{d_4}} \exp\left\{-\left(d_1A + d_2A^2 + d_3A^3\right)\right\} \tag{21}$$

Here, $\{A|0 < A < \infty\}$, and C denotes a normalization constant. To determine the coefficients d_1, d_2, d_3, d_4 of Eq. (21), the moment values of the roll amplitude are used as a constraint condition. As mentioned above, the even-order moment values of the roll amplitude can be derived from Eqs. (18) to (20). However, the odd-order moment values are not easily derived. The following approach is carried out to overcome this problem. If the PDF is symmetric, the odd-order moment values are all zero. However, the roll amplitude is a positive value. In other words, if the PDF in Eq. (21) is used, this approach cannot be applied. To use this approach, a new PDF such as Eq. (22) is defined based on the PDF of the roll amplitude expressed in Eq. (21).

$$\mathcal{P}(\bar{A}) = \frac{C'}{|\bar{A}|^{d_4}} \exp\left\{-\left(d_1|\bar{A}| + d_2|\bar{A}|^2 + d_3|\bar{A}|^3\right)\right\} \tag{22}$$

Here, $\{\bar{A}| -\infty < \bar{A} < \infty\}$ and C' denotes the normalization constant, whereby $C = 2C'$ holds. The function of Eq. (22) is an even function. Thus, all odd-order moment values are equal to zero. Thereby, the problem of deriving the odd-order moment values is overcome. In other words, using our proposed PDF of Eq. (22) and the even-order moment values of the roll amplitude, the coefficients d_1, d_2, d_3, d_4 can be determined. In addition, the objective function of Eq. (23) is defined as

$$J\left(d_1, d_2, d_3, d_4\right) = \sum_{i=1}^{6} l_i |J_i| \tag{23}$$

where

$$J_i = \int_{-\infty}^{+\infty} \bar{A}^i \mathcal{P}(\bar{A})\, \mathrm{d}\bar{A} - \mathbb{E}\left[\bar{A}^i\right] \tag{24}$$

Here, l_i are weights and $l_i = 1\,(i = 1, 2, ..., 6)$. In this study, moments up to the sixth-order are used for the determination of the coefficients (Appendix 2). In Eq. (24), the even-order moment values of $\bar{A}$ are derived from Eqs. (18) to (20). On the other hand, the odd-order moment values of $\bar{A}$ are all zero.

Table 4 Initial values for the calculation of the moment equations

	$\mathbb{E}\left[X_1^2\right]$ and $\mathbb{E}\left[X_2^2\right]$	$\mathbb{E}\left[X_2^4\right]$ and $\mathbb{E}\left[X_2^4\right]$	otherwise
2nd-order	0.01	–	0.01
3rd-order	0.01	–	0
4th-order	0.01	0.0001	0

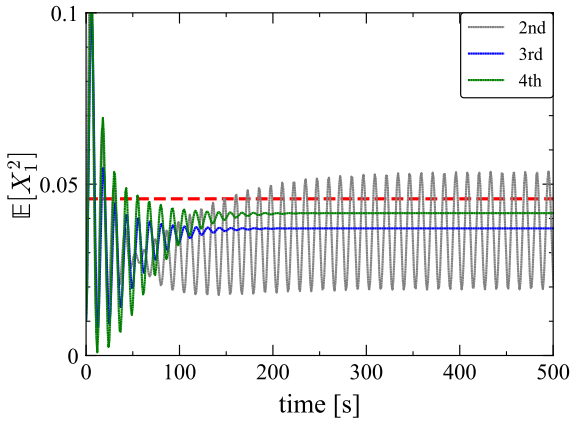

Fig. 7 Displacement of $\mathbb{E}\left[X_1^2\right]$ obtained by computing the moment equations. Here, the 2nd-, 3rd-, and 4th-order cumulant neglect closure methods are used. The red dotted line shows the MCS result in Table 5

6 Calculation results

In this study, the subject ship is the C11 container vessel. The corresponding calculation results are compared for the Froude number Fn = 0.00 in head seas. Note that the choice of this Froude number leads to severe parametric rolling conditions. The MCS result is obtained by solving the SDE (Eq. (13)). In this numerical calculation, the Euler-Maruyama method [37] is used. The time step is 0.001 s, and the initial condition is set to a roll angle of 5 deg and a roll rate of 0 deg/s. The number of realizations is 1000 and each numerical simulation time is 1 h. Thereby, the PDF of the roll amplitude, which is plotted with ∘ in Fig. 8, is obtained. In this figure, the vertical axis of the left panel has a linear scale, while the vertical axis of the right panel has a logarithmic scale. From this PDF, the even-order moment values of roll amplitude are derived in Table 6. Moreover, the even-order moment values of the roll angle, roll rate, and effective wave elevation are obtained in Table 5.

Table 5 Moment values obtained from the MCS and by solving the moment equations, with Fn = 0.00

	MCS	Moment eq. (2nd)	Moment eq. (3rd)	Moment eq. (4th)
$\mathbb{E}\left[X_1^2\right]$	4.57×10^{-2}	3.64×10^{-2}	3.71×10^{-2}	4.15×10^{-2}
$\mathbb{E}\left[X_1^4\right]$	5.84×10^{-3}	3.98×10^{-3}	4.13×10^{-3}	5.44×10^{-3}
$\mathbb{E}\left[X_2^2\right]$	2.93×10^{-3}	2.37×10^{-3}	2.41×10^{-3}	2.65×10^{-3}
$\mathbb{E}\left[X_2^4\right]$	2.42×10^{-5}	1.68×10^{-5}	1.74×10^{-5}	2.11×10^{-5}
$\mathbb{E}\left[X_3^2\right]$	0.818	0.815	0.815	0.815
$\mathbb{E}\left[X_3^4\right]$	2.00	1.99	1.99	1.99

Table 6 Moment values of the roll amplitude obtained from the MCS and by using Eqs. (18) to (20), with Fn = 0.00

	MCS	Moment eq. (2nd)	Moment eq. (3rd)	Moment eq. (4th)
$\mathbb{E}\left[A^2\right]$	9.17×10^{-2}	7.43×10^{-2}	7.56×10^{-2}	8.40×10^{-2}
$\mathbb{E}\left[A^4\right]$	1.57×10^{-2}	1.10×10^{-2}	1.14×10^{-2}	1.45×10^{-2}
$\mathbb{E}\left[A^6\right]$	3.75×10^{-3}	2.46×10^{-3}	2.59×10^{-3}	3.87×10^{-3}

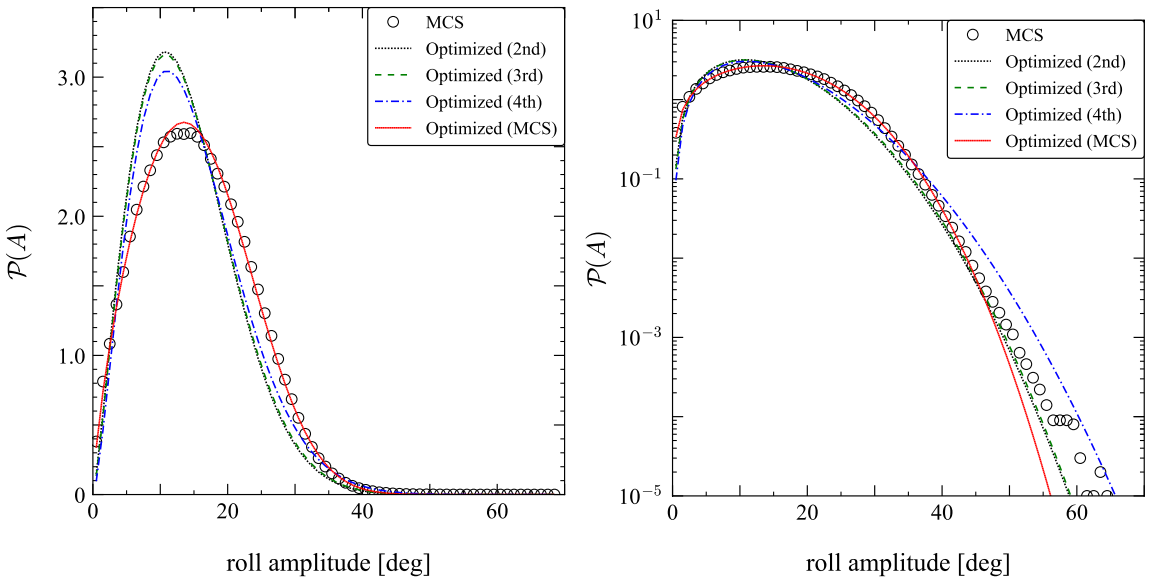

Fig. 8 Comparison of the PDFs of the roll amplitude among the MCS result and the optimized results by using the moment values (Table 6), with Fn =0.00

Next, the moment values are computed by using the moment equations (Eq. (15)) and the cumulant neglect closure method. The moment equations of Eq. (15) are ordinary differential equations. In this study, these moment equations are calculated in an unsteady state ($\frac{\mathrm{d}}{\mathrm{d}t}\mathbb{E}[\cdot] \neq 0$). For this, the 4th-order Runge–Kutta method is used, where the time step is set to 1 s. As the time step becomes smaller, the amount of data increases. As a result, the calculation time increases. On the other hand, if the time step is too large, it may not be possible to obtain a solution due to numerical problems. This was already proposed by Maruyama et al. [18]. The used initial condition are shown in Table 4.

As an example, the time series of the displacement of $\mathbb{E}\left[X_1^2\right]$, which is obtained by solving the moment equations numerically, is shown in Fig. 7.

This figure shows the plots for the calculation results of the 2nd, 3rd, and 4th-order moment equations (gray, blue, and green lines, respectively). Furthermore, the red dashed line denotes the moment value obtained from the MCS result.

In Fig. 7, it can be clearly observed that the numerical solution of the moment equations up to 2nd-order are oscillatory in the steady state. On the other hand, the numerical solution of the 3rd- and 4th-order moment equations are non-oscillatory in the steady state. The moment

values obtained from moment equations are derived by averaging the displacements in the steady state and are shown in Table 5. The 4th-order moment values of X_1, X_2, and X_3 with respect to "Moment eq.(2nd)" and "Moment eq.(3rd)" of Table 5 are computed by using the 2nd- and 3rd-order cumulant neglect closure method, respectively. On the other hand, the 4th-order moment values with respect to "Moment eq.(4th)" of Table 5 can be directly obtained from the moment equations. It can be seen from Fig. 7 and Table 5 that when higher-order moment equations are used, the resulting moment values approach the results from numerical simulations more closely.

The moment values of the roll amplitude are shown in Table 6. These moment values can be obtained by substituting the moment values of Table 5 in Eqs. (18) to (20). From the used moment equations, the result of "Moment eq.(4th)" is closest to the MCS result. In other words, when the moment values of the roll amplitude are computed using the higher-order moment equations, the resulting moment values are closer to the MCS result.

The PDF of the roll amplitude is derived based on the moment values of the roll amplitude in Table 6 and Eqs. (21) to (23). The result of the roll amplitude PDF is shown in Fig. 8. Here, ∘ denotes the MCS result. Furthermore, this figure shows the results obtained by applying the moment values of "Moment eq.(2nd)", "Moment eq.(3rd)", "Moment eq.(4th)", "MCS" in Table 6 to Eq. (24) (black dotted, green dashed, blue dashed-dotted, red solid lines, respectively). It can be clearly observed that the PDF of "Optimized (4th)" is closer to the MCS result than the PDFs of "Optimized (2nd)" and "Optimized (3rd)." However, this PDF does not agree with the MCS result. The reason for this discrepancy is that the moment values of "Moment eq.(4th)" in Table 6 do not agree with the moment values of the MCS result. To determine other causes, the appropriateness of the PDF shape proposed in Eq. (21) is examined by using the moment values of "MCS" from Table 6 in Eq. (24). As shown in Fig. 8, the PDF of "Optimized (MCS)" overlaps with the MCS result. Therefore, it is clear that using the appropriate moment values in the objective function and applying our proposed PDF, the PDF of the roll amplitude, which agrees with the MCS result, can be derived.

7 Conclusions

It has been shown that an effective wave can be generated even when a 4th-order linear filter is used. However, the 6th-order ARMA spectrum is in better agreement with the theoretical spectrum than the 2nd and 4th-order ARMA spectrum. In addition, the modeling of waves with a 6th-order linear filter is more accurate than with a 2nd and 4th-order linear filter.

In this study, the moment equations have been derived from a 6th-order SDE. In the calculation, the moment values of the roll angle, roll rate, and effective wave elevation are obtained by applying the cumulant neglect closure method. The moment values obtained by applying the 2nd-, 3rd-, and 4th-order cumulant neglect closure methods have been compared and it can be observed that the resulting moment values are close to the MCS result when the higher-order cumulant neglect closure method is applied.

Furthermore, we proposed a method for deriving the moment values of the roll amplitude by combining the linearity of expectation and the moment values related to the roll angle and roll rate. The results showed that the even-order moment values of the roll amplitude can be obtained by our proposed method. Additionally, a method was proposed for deriving the PDF of the roll amplitude by using the moment values of the roll amplitude and our proposed PDF. It was shown that the PDF of the roll amplitude agrees well with the MCS result if the appropriate moment values are used. It is to be noted that the method for deriving the moment values of the roll amplitude and our proposed PDF were both reasonable.

This study showed that the PDF of the roll amplitude can be obtained using the moment equation. In future, the applicability of our proposed method will be analysed by changing the calculation conditions, such as subject ships, sea conditions, and ship speed. Other PDF shapes should also be investigated.

Appendix 1

In general, the position where the white noise is added in the linear filter is set as Eqs. (1) to (3). The expression of the numerator in the ARMA spectrum is different depending on the added position of the white noise; however, the added position of the white noise has no effect on the expression of the denominator. In this appendix, we investigate how the added position of the white noise affects fitting the ARMA spectrum to the theoretical spectrum, generating the time series, and the PDF.

The relationship between the added position of the white noise and the output is computed based on the 6th-order linear filter. First, the ordinary differential equation of the 6th-order linear filter is represented as Eq. (25), with the notation for differentiation being represented by Lagrange's notation.

$$x_1^{(6)} + \alpha_1 x_1^{(5)} + \alpha_2 x_1^{(4)} + \alpha_3 x_1''' + \alpha_4 x_1'' + \alpha_5 x_1' + \alpha_6 x_1 = \Gamma\sqrt{\pi}\{W'\}^{(n)} \quad (n = 0, \ldots, 5) \tag{25}$$

where W' denotes white noise. The relationship between the added position of the noise and n in Eq. (25) is shown in Eq. (26). In this case, $n = 0, \ldots, 5$ denotes the hierarchy to add the white noise.

$$\begin{cases} \dfrac{dx_1}{dt} = x_2 - \alpha_1 x_1 & \leftarrow n = 5 \\ \dfrac{dx_2}{dt} = x_3 - \alpha_2 x_1 & \leftarrow n = 4 \\ \dfrac{dx_3}{dt} = x_4 - \alpha_3 x_1 & \leftarrow n = 3 \\ \dfrac{dx_4}{dt} = x_5 - \alpha_4 x_1 & \leftarrow n = 2 \\ \dfrac{dx_5}{dt} = x_6 - \alpha_5 x_1 & \leftarrow n = 1 \\ \dfrac{dx_6}{dt} = -\alpha_6 x_1 & \leftarrow n = 0 \end{cases} \tag{26}$$

Next, the Laplace transform of Eq. (26) yields Eq. (27).

$$\left(s^6 + s^5\alpha_1 + s^4\alpha_2 + s^3\alpha_3 + s^2\alpha_4 + s\alpha_5 + \alpha_6\right)X_1(s) = \Gamma s^n \sqrt{\pi} U(s) \quad (n = 0, \ldots, 5) \tag{27}$$

Here, $U(s)$ and $X_1(s)$ denote the Laplace transform of the input and the output, respectively. The transfer function can be derived as Eq. (28).

$$\mathcal{H}_6(s) = \frac{\Gamma s^n \sqrt{\pi}}{s^6 + s^5\alpha_1 + s^4\alpha_2 + s^3\alpha_3 + s^2\alpha_4 + s\alpha_5 + \alpha_6} \quad (n = 0, \ldots, 5) \tag{28}$$

Furthermore, using $s = i\omega$, the 6th-order ARMA spectrum can be obtained as Eq. (29).

$$S_6(\omega) = \frac{\Gamma^2 \omega^{2n}}{\left(-\omega^6 + \alpha_2\omega^4 - \alpha_4\omega^2 + \alpha_6\right)^2 + \left(\alpha_1\omega^5 - \alpha_3\omega^3 + \alpha_5\omega\right)^2} \quad (n = 0, \ldots, 5) \tag{29}$$

Figure 9 shows the ARMA spectrum for each added position of the noise. Using the obtained coefficients α_i, Γ and numerically solving the SDE corresponding to Eq. (25), the time series of wave elevation can be obtained. Figure 11 is shown as an example. In this calculation, the same input data are used for all added positions of the noise. Furthermore, as shown in Fig. 10, the PDFs of wave elevation are obtained from the obtained time series. It can be seen that the result for $n = 5$ has a slight discrepancy compared to the other results when the wave elevation is small. Figure 11 shows that the time series of $n = 5$ is noisier than other time series. We assume that this is because of the white noise added to the hierarchy of output. However, the obtained PDFs of the wave elevation are equal, and there is no excessive discrepancy among these PDFs, irrespective of where the noise is added or not.

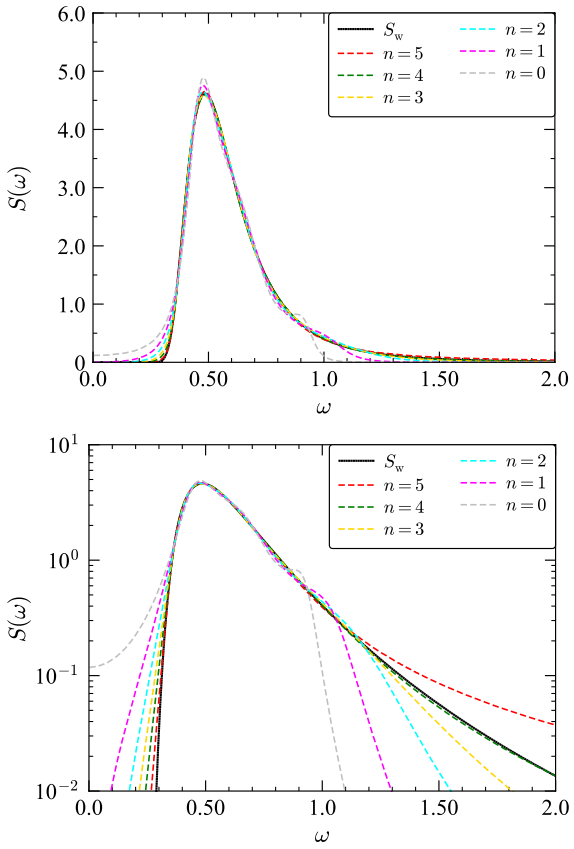

Fig. 9 Comparison of spectra among $n = 0, \ldots, 5$ and ITTC spectrum, sea state with $T_{01} = 9.99$ s and $H_{1/3} = 5.0$ m

The time series of the wave elevation obtained by using the same input data is shown in Fig. 11. The lower panel in Fig. 11 is the extended figure of the upper panel in Fig. 11. As shown in the lower panel, a phase difference occurs for each added position of noise. This phase difference is discussed based on the Bode plot shown in Fig. 13. This Bode plot is generated using the transfer function represented by Eq. (28). The red line in Eq. (28) denotes the peak value ω_p of the ITTC spectrum. This value is derived from Eq. (30). Thereby, when T_{01} is 9.99 s, $\omega_p = 0.485$.

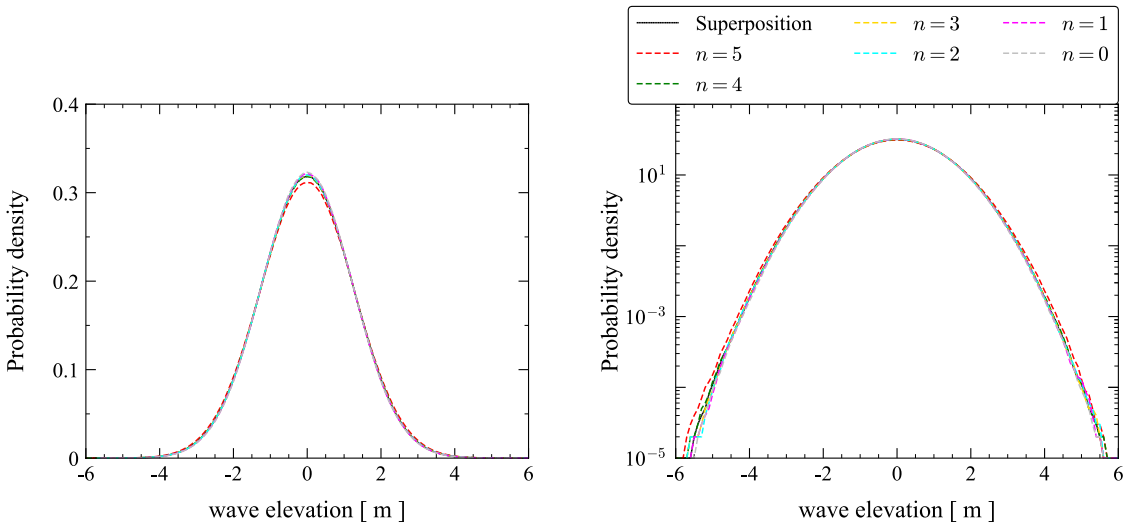

Fig. 10 Comparison of wave elevation PDFs among $n = 0, \ldots, 5$ and numerical simulation by superposition methodology: Superposition

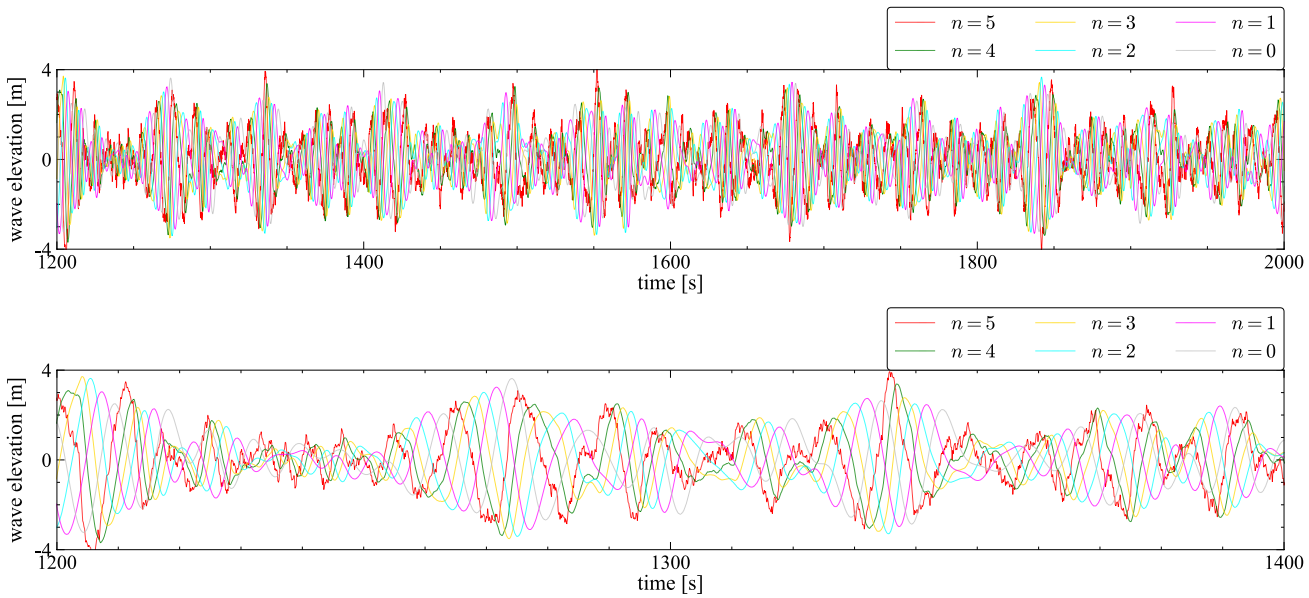

Fig. 11 Comparison of time series of wave elevation among $n = 0, \ldots, 5$

$$\omega_{\mathrm{p}} = \sqrt[4]{0.8B_{\mathrm{w}}} \tag{30}$$

where

$$B_{\mathrm{w}} = \frac{691}{T_{01}^4} \tag{31}$$

The phase of each added position of the noise in ω_{p} is shown in the first line of Table 7. In addition, the phase difference with respect to $n = 5$ is shown in the second line of Table 7. The peak period obtained from $\omega_{\mathrm{p}} = 0.485$ is 12.9 s. Based on this period, the third line of Table 7 is obtained by converting the phase difference to time difference. Thereby, by shifting the time series in Fig. 11 to just these time differences, the corrected time series shown in Fig. 12 is obtained. Compared to the original time series, the corrected time series all overlap. As mentioned above, the original time series is generated by using the same white noise data. Thereby, the time series of the output has almost the same period and wave amplitude.

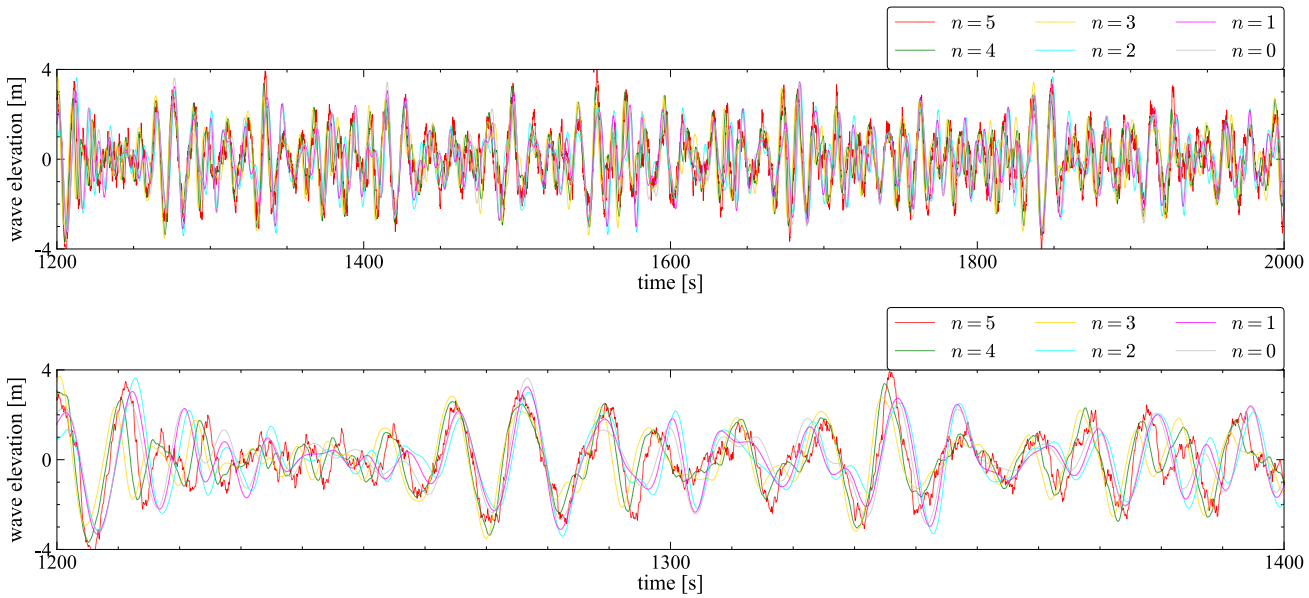

Fig. 12 Comparison of time series of wave elevation among $n = 0, \ldots, 5$ after correcting the phase

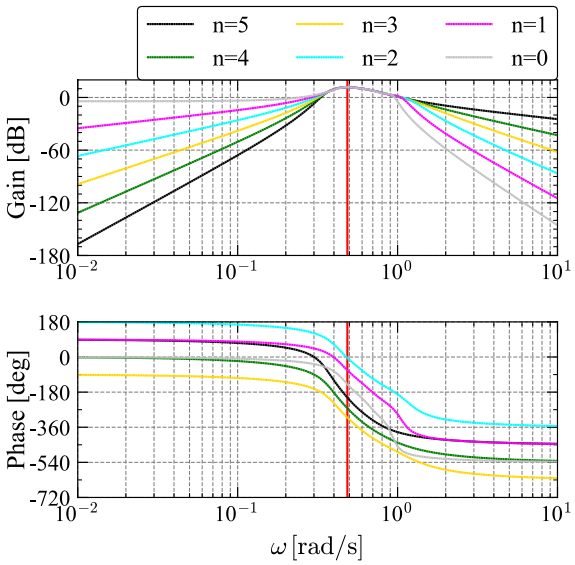

Fig. 13 Bode plot

In the resulting time series, the differences in smoothness and the phase difference occur depending on the position of the white noise. However, no matter where the noise is added, we can see that the time series is not very incorrect. Therefore, white noise can be added to any hierarchy. When the white noise is added to the middle hierarchy such as $n = 2$ or 3, the fitting of the ARMA spectrum to the ITTC spectrum and the modeling of the time series are satisfied overall. Therefore, the white noise should be added to $n = 2$ or 3 unless there is a specific reason not to do so.

Appendix 2

The objective function, which is used to determine the coefficients d_1, d_2, d_3, d_4 included in Eqs. (21) and (22), is discussed here. In this objective function, the moment values are used as the constraint conditions. We need to investigate the maximum order up to which the moment values need to be used. When the PDF is derived, the statistical indices, such as mean, variance, skewness, and kurtosis, should be considered. Therefore, the minimum requirement is to use up to 4th-order moment values. In this study, the four types of $n = 4, 6, 8, 10$ in Eq. (32) are set and the calculation result is considered. Using the equation

Table 7 Phase of $n = 0, \ldots, 5$ at ω_p, phase and time difference with respect to phase of $n = 5$

	$n = 5$	$n = 4$	$n = 3$	$n = 2$	$n = 1$	$n = 0$
Phase [deg]	−208	−262	−310	−4.19	−67.6	−139
Phase difference [deg]	0.00	−54.5	−102	203	140	68.4
Time difference [s]	0.00	−1.96	−3.68	7.31	5.03	2.46

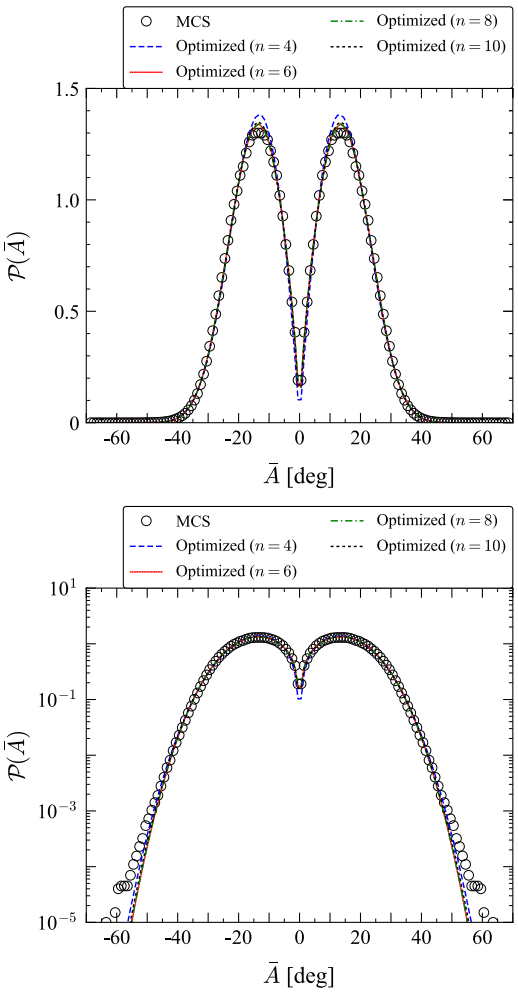

Fig. 14 Comparison of several optimized PDFs by using Eq. (22) and the MCS result, with C11 and $Fn = 0.00$

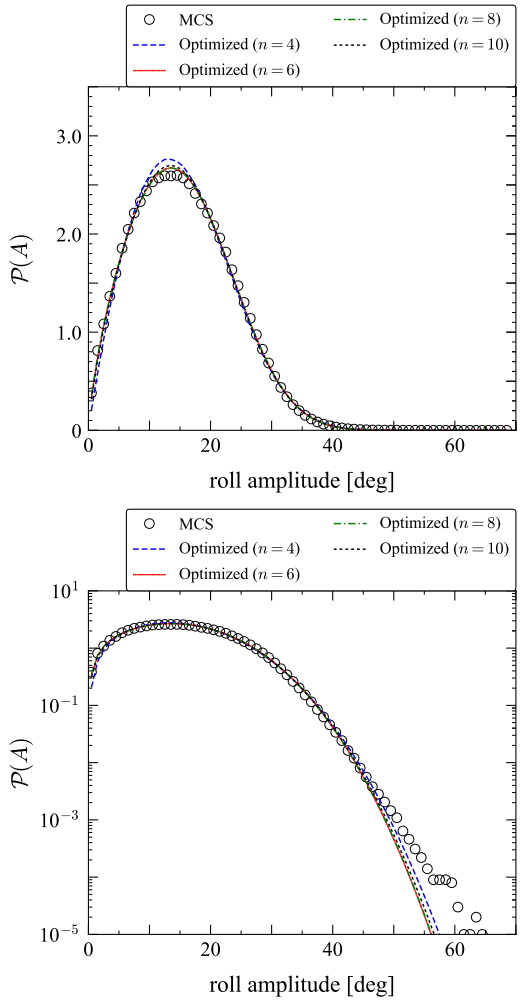

Fig. 15 Comparison of several optimized PDFs by using Eq. (21) and the MCS result, with C11 and $Fn = 0.00$

$$J(d_1, d_2, d_3, d_4) = \sum_{i=1}^{n} l_i |J_i|, \tag{32}$$

the values $n = 4, 6, 8, 10$ are selected in this study.

In this equation, l_i are weights and J_i is represented by Eq. (24), and the moment values used as the constraint conditions apply the values of "MCS" in Table 6. In addition, the l_i values are all set to 1.

The optimized PDFs represented by Eq. (22) are shown in Fig. 14. Also, based on the resulting coefficients, the PDF of the roll amplitude represented by Eq. (21) is shown in Fig. 15. From Figs. 14 and Fig. 15, it is clear that the result for $n = 4$ is not appropriate. The moment values obtained

Table 8 Comparison of moment values obtained from several optimized PDFs and the MCS result

	MCS	$n = 4$	$n = 6$	$n = 8$	$n = 10$
$\mathbb{E}[X^2]$	9.17×10^{-2}	9.17×10^{-2}	9.17×10^{-2}	9.17×10^{-2}	9.17×10^{-2}
$\mathbb{E}[X^4]$	1.57×10^{-2}	1.57×10^{-2}	1.57×10^{-2}	1.57×10^{-2}	1.57×10^{-2}
$\mathbb{E}[X^6]$	3.75×10^{-3}	3.80×10^{-3}	3.75×10^{-3}	3.75×10^{-3}	3.76×10^{-3}
$\mathbb{E}[X^8]$	1.13×10^{-3}	1.16×10^{-3}	1.12×10^{-3}	1.12×10^{-3}	1.13×10^{-3}
$\mathbb{E}[X^{10}]$	4.10×10^{-4}	4.22×10^{-4}	3.94×10^{-4}	3.94×10^{-4}	4.03×10^{-4}

Table 9 Evaluation of the optimized PDFs with $n = 4, 6, 8, 10$ as shown in Fig. 14

	Mean squared error
$n = 4$	4.93×10^{-3}
$n = 6$	8.55×10^{-4}
$n = 8$	8.10×10^{-4}
$n = 10$	1.47×10^{-3}

from the optimized PDF are shown in Table 8. In addition, based on the MCS result and the optimized PDF, the estimation results obtained by using the mean squared error are shown in Table 9. Here, the MCS result represents the true value, and the optimized PDF the measured value. Considering the results of Fig. 14 and Tables 8 and 9, $n = 6$ is the appropriate value for deriving the PDF of roll amplitude. Therefore, $n = 6$ is used in this study.

Acknowledgements The authors would like to thank Prof. Umeda, N. in Osaka University for useful discussions. This work was supported by a Grant-in-Aid for Scientific Research from the Japan Society for Promotion of Science (JSPS KAKENHI Grant Number 19H02360) and by Support for Pioneering Research Initiated by the Next Generation from Japan Science and Technology Agency (JST SPRING, Grant Number JPMJSP2138), as well as the collaborative research program / financial support from the Japan Society of Naval Architects and Ocean Engineers. This study was supported by the Fundamental Research Developing Association for Shipbuilding and Offshore (REDAS), managed by the Shipbuilders' Association of Japan from April 2020 to March 2023.

Funding Open Access funding provided by Osaka University.

References

1. France WN, Levadou M, Treakle TW, Paulling JR, Michel RK, Moore C (2003) An investigation of head-sea parametric rolling and its influence on container lashing systems. Marine Technol SNAME News 40(1):1
2. IMO (2004), Review of the intact stability code - recordings of head sea parametric rolling on a pctc., SLF 47/INF.5 pp. 37 – 40
3. Rosén A, Huss M, Palmquist M (2012) Experience from parametric rolling of ships, Parametric resonance in dynamical systems pp. 147 – 165
4. IMO, Interim guidelines on the second generation intact stability criteria., MSC.1/Circ 1627 pp. 1 – 60 (2020)
5. IMO, Simplified operational guidance from level 2 vulnerability assessment for parametric roll., SDC 8/WP.4/Add.5 pp. 37 – 40 (2022)
6. Hashimoto H, Umeda N (2004) Nonlinear analysis of parametric rolling in longitudinal and quartering seas with realistic modeling of roll-restoring moment. J Marine Sci Technol 9:117
7. Sakai M, Umeda N, Yano T, Maki A, Yamashita N, Matsuda A, Terada D (2018) Averaging methods for estimating parametric roll in longitudinal and oblique waves. J Marine Sci Technol 23(3):413
8. Maki A, Umeda N, Shiotani S, Kobayashi E (2011) Parametric rolling prediction in irregular seas using combination of deterministic ship dynamics and probabilistic wave theory. J Marine Sci Technol 16:294
9. Ariaratnam ST, Tam DSF (1979) Random vibration and stability of a linear parametrically excited oscillator. Zeitschrift Angewandte Mathematik und Mechanik 59:79
10. Roberts JB (1982) Effect of parametric excitation on ship rolling motion in random waves. J Ship Res 26(4):246
11. Stratonovich RL (1963) Topics in the theory of random noise. In: Mathematics and its applications, Gordon and Breach
12. Khas'minskii RZ (1966) A limit theorem for the solutions of differential equations with random right-hand sides. Theory Probab Appl 11(3):390
13. Roberts J (1977) Stationary response of oscillators with non-linear damping to random excitation. J Sound Vib 50(1):145
14. Roberts JB (1982) A stochastic theory for nonlinear ship rolling in irregular seas. J Ship Res 26(4):229
15. Roberts J, Spanos P (1986) Stochastic averaging: An approximate method of solving random vibration problems. Int J Non-Linear Mech 21(2):111
16. Dostal L, Kreuzer E, Sri Namachchivaya N (2012) Non-standard stochastic averaging of large-amplitude ship rolling in random seas., Proceedings: Mathematical. Phys Eng Sci 468(2148):4146
17. Maruyama Y, Maki A, Dostal L, Umeda N (2022) Improved stochastic averaging method using hamiltonian for parametric rolling in irregular longitudinal waves. J Marine Sci Technol 27(1):186
18. Maruyama Y, Maki A, Dostal L, Umeda N (2022) Application of linear filter and moment equation for parametric rolling in irregular longitudinal waves. J Marine Sci Technol 27:1252–1267
19. Hashimoto H, Umeda N (2010), A study on quantitative prediction of parametric roll in regular waves., Proceedings of the 11th International Ship Stability Workshop, Wageningen, The Netherlands pp. 295 – 301
20. Hamamoto M, Kim Y, Uwatoko K (1991) Study on ship motions and capsizing in following seas (final report). J Soc Naval Arch Jpn 1991(170):173
21. Kawahara Y, Maekawa K, Ikeda Y (2012) A simple prediction formula of roll damping of conventional cargo ships on the basis of ikeda's method and its limitation. J Ship Ocean Eng 2(4):201
22. Spanos PTD (1983) ARMA Algorithms for Ocean Wave Modeling. J Energy Resources Technol 105(3):300
23. Spanos PT (1986) Filter approaches to wave kinematics approximation. Appl Ocean Res 8(1):2
24. Flower J, Vijeh N (1983) A note on ratio-of-polynomials curve-fitting of seawave spectra. Int Shipbuilding Progress 30(341):10
25. Flower J, Vijeh N (1985) Further considerations of the ratio-of-polynomials form-fit of seawave spectra. Int Shipbuilding Progress 32(365):2
26. Thampi SK, Niedzwecki JM (1992) Filter approach to ocean structure response prediction. Appl Ocean Res 14(4):259
27. Grim O (1961) Beitrag zu dem problem der sicherheit des schiffes in seegang. Schiff und Hafen 6:490–497
28. Umeda N, Ariji M, Yamakoshi Y (1991) Assessment for probability of ship capsizing due to pure loss of stability in quartering seas (2nd report). J Kansai Soc Naval Arch Jpn 216:129
29. Hansen N (2006) The CMA Evolution Strategy: A Comparing Review. Springer, Berlin Heidelberg
30. K. Sobczyk (1991), *Stochastic Differential Equations With Applications to Physics and Engineering*. Mathematics and Its Applications. (Springer Netherlands,)
31. Wong E, Zakai M (1965) On the relation between ordinary and stochastic differential equations. Int J Eng Sci 3(2):213
32. Sun J.Q, Hsu C.S (1987) Cumulant-neglect closure method for nonlinear systems under random excitations. J Appl Mech 54(3):649

33. Sun J.Q (1989) Cumulant-neglect closure method for asymmetric non-linear systems driven by gaussian white noise. J Sound Vib 135(2):338
34. Wojtkiewicz S.F, Spencer B.F, Bergman L.A (1996) On the cumulant-neglect closure method in stochastic dynamics. Int J Non-Linear Mech 31(5):657
35. Hashimoto H, Umeda N, Matsuda A, Nakamura S(2006) Experimental and numerical study on parametric roll of a post-panamax container ship in irregular waves, Proceedings of the 9th International Conference on the Stability of Ships and Ocean Vehicles (STAB 2006)
36. Maki A, MaruyamaY, Umeda N, Miino Y, Katayama T, Sakai M, Ueta T (2019) A perspective on theoretical estimation of stochastic nonlinear rolling., Proceedings of the 17th International Ship Stability Workshop, Helsinki, Finland pp. 39 – 46
37. Maruyama G (1955) Continuous Markov processes and stochastic equations. Rendiconti del Circolo Matematico di Palermo 4(1):48